Journal of Molecular Catalysis A: Chemical xxx (2016) xxx–xxx

Contents lists available at ScienceDirect

Journal of Molecular Catalysis A: Chemical

journal homepage: www.elsevier.com/locate/molcata

Decomposition of acetic acid for hydrogen production over Pd/Al_2O_3 and Pd/TiO_2: Influence of metal precursor

Laura M. Esteves, Maria H. Brijaldo, Fabio B. Passos*

Departamento de Engenharia Química e de Petróleo, Universidade Federal Fluminense, Niterói, RJ, Brazil

ARTICLE INFO

Article history:
Received 1 October 2015
Received in revised form 30 January 2016
Accepted 1 February 2016
Available online xxx

Keywords:
Hydrogen
Palladium
Decomposition
Acetic acid
Precursor effect
Support effect

ABSTRACT

The effect of palladium precursor on the catalytic properties of Pd/Al_2O_3 and Pd/TiO_2 catalysts toward acetic acid decomposition was investigated. The catalysts were prepared by incipient wetness impregnation of titania and alumina with solutions of palladium acetylacetonate, palladium chloride and palladium nitrate. All the catalysts were characterized by N_2-physisorption, XRD, H_2-TPR, H_2-chemisorption, XPS and IR spectroscopy (DRIFTS *in situ*). Carbonaceous compounds were formed on the used catalysts and were investigated by TPO, TGA experiments and Raman spectroscopy. The results suggested that Pd/Al_2O_3 Nit (prepared using palladium nitrate) was the most active catalyst for conversion of acetic acid, followed by Pd/Al_2O_3 Aca (prepared using palladium acetylacetonate) which was the most selective for H_2. Alumina supported catalysts showed the best performance in acetic acid decomposition and hydrogen production.

1. Introduction

The global growing energy consumption, the pollution caused by conventional energy production technologies and the world's population growth have resulted in a quest for alternative and renewable energy sources, including biomass [1]. The utilization of lignocellulosic waste, such as forest residues and sawdust, is especially sustainable and economically attractive because this feedstock does not compete with food production [2]. For instance, bio-oil derived from fast pyrolysis of biomass can be applied to hydrogen production. Today, hydrogen is one of the most widely investigated alternative energy carrier, due to its several environmental advantages [3]. There are many ways to produce hydrogen, but not all of them are a compromise between hydrogen economy and environmental safety. Nowadays, hydrogen is mainly produced at industrial scale by steam reforming of natural gas and naphtha, partial oxidation of heavy residual oils or coal gasification. All these feedstocks are fossil fuels derived, and thus they contribute for the increased emissions of greenhouse gases [4]. In order to reduce these emissions, hydrogen production from bio-oil derived from fast pyrolysis of biomass is an alternative for its production and consequent application in fuel cells [5].

Fast pyrolysis is a process in which biomass is rapidly heated to high temperatures in the absence of oxygen. As result, biomass decomposes to generate vapor, bio-oil and charcoal. The composition of bio-oil differs with the type of biomass and the conditions of pyrolysis [5]. The condensation of these gases leads to a bio-oil and it can be divided into two fractions: an aqueous phase and a non-aqueous phase. The aqueous fraction consists of a range of oxygenate compounds, which can be potential renewable sources of hydrogen. Due to the amount of oxygenate compounds found in the aqueous fraction, model compounds have usually been used to investigate possible pathways and trends when converting bio-oil at laboratorial scale. Acetic acid is one of the most popular compounds used to represent the aqueous fraction of bio-oil [6] and one of the major components in bio-oil (up to 19%) [6,7]. Nickel, other transition metals and noble metals such as palladium, and different supports (Al_2O_3, ZrO_2, MgO, *etc.*) have already been tested in several reactions like the steam reforming of acetic acid [7–10]. The main disadvantage of this process is the high formation of carbonaceous deposits on the catalyst surfaces causing the loss of activity.

The decomposition of acetic acid may produce a mixture of carbon monoxide and hydrogen according to the following chemical reaction:

$$CH_3COOH \rightarrow 2CO + 2H_2 \quad (1)$$

* Corresponding author at: Rua Passo da Pátria, 156. São Domingos, Niterói 24210-240, Brazil. Fax: +55 2126295368.
E-mail addresses: lauraesteves@id.uff.br (L.M. Esteves), mh_brijaldo@id.uff.br (M.H. Brijaldo), fbpassos@vm.uff.br, fabiopassos@id.uff.br (F.B. Passos).

http://dx.doi.org/10.1016/j.molcata.2016.02.001
1381-1169/

The literature on decomposition of acetic acid to hydrogen production is scarce [11–17] and its investigation may lead to a better understanding of activity–structure correlations that could help to optimize bio-oil conversion. For the conversion of acetic acid and other carboxylic acids over metal supported catalysts acetate species plays an important role as an intermediate. Acetic acid decomposes to form acetate, liberating hydrogen and also produce CO_2 and C [13,14].

Bowker et al. [13] studied acetic acid adsorption and decomposition on Pd (110) using temperature-programmed desorption (TPD). They found the adsorption of acetic acid was efficient and hydrogen and acetate formation occurred at room temperature. The acetate decomposed between 47 °C and 167 °C to form CO_2 and hydrogen and left carbon adsorbed on the surface. Acetate was unstable at higher temperatures (>177 °C), but adsorption of acetic acid continued at a steady-state rate and was not poisoned by the buildup of carbon on the crystal. This was due to the fact that most of the carbon deposited was lost from the surface to the bulk in a facile manner above about 177 °C, therefore leaving a reactive surface that was apparently continuously available for acetic acid decomposition. In other studies, H_2 was observed on Rh(110) [14], while a combination of CO, CO_2, H_2, and H_2O was reported on Rh(111) [15]. Scharpf and Benziger [16] studied the decomposition of acetic acid monomer an dimer on Ni(100). After acetic acid monomer adsorbed molecularly at −103 °C, the acid hydrogen was irreversibly lost at −33 °C and bridge-bounded acetate was formed which then underwent a reversible transformation to a monodentate acetate above 47 °C and after that eventually decomposed to CO_2, C (ad) and H_2 at 162 °C. The authors found that the key step in acetate decompositions is the C–C scission. In other study, Madix et al. [17] also investigated the acetic acid decomposition on Ni(110). Acetic acid adsorbed at 30 °C yielded gaseous H_2O and formed islands of adsorbed anhydride intermediates. In their work the decomposition products were H_2, CO_2, CO, H_2 and surface carbon. Besides, the decomposition of the anhydride was rate determining for the formation of CO_2 and H_2.

The choice of support may influence the reaction pathways, including intermediates, and product selectivity in carboxylic acid formation [18]. Different types of metal–support interactions may occur and these interactions can have a significant effect in determining catalytic activity and selectivity. In a recent work, Brijaldo et al. [19] studied the acetic acid decomposition over Pd/SiO_2, Pd/Nb_2O_5, Pd/La_2O_3 and Pd/Fe_2O_3 for hydrogen production. The products of acetic acid decomposition were H_2, CO, CH_4, CO_2, H_2O and C_2H_4O. Hydrogen was only observed at temperatures above 600 °C. Pd/Fe_2O_3 was the most active catalyst for conversion of acetic acid and showed high hydrogen selectivity and good catalytic stability. The Pd/Fe_2O_3 catalyst exhibited good catalytic stability during acetic acid decomposition followed by Pd/Nb_2O_5, Pd/La_2O_3 and Pd/SiO_2. The excess of active sites turned Pd/Fe_2O_3 to the most active catalyst and the carbon type found after the reaction corresponded to a highly ordered carbon. Despite the mentioned investigations, there are not systematic studies about the effect of the precursor and the support on acetic acid decomposition over supported metal catalysts. Therefore, in this work, the decomposition of acetic acid was carried out using palladium supported catalysts [20]. Palladium active sites are influenced by several factors, such as particle metal size, metal-support interaction and nature of precursor salts [21]. For palladium catalysts, metal precursors are usually chlorides or other inorganic salts [22]. Different supports have been widely used to prepare palladium catalysts, like Al_2O_3 and TiO_2. These supports have different characteristics: Al_2O_3 is an acid and non-reducible support, while TiO_2 is a typical reducible support [23]. The influence of the support has been studied in the literature [24,25] and it was concluded that the nature of the support plays an important role in the palladium–support interaction. The use of different palladium precursors has also been reported in literature as an important factor to obtain good dispersion of palladium on the surface of the supports [26,27] to improve the catalytic activity.The main goal of this work was to determine the effect of different palladium precursors and supports on the reactivity of palladium supported catalysts for decomposition of acetic acid. For this purpose, alumina and titania supported palladium catalysts were prepared using different palladium precursors (chloride, acetylacetonate and nitrate). The prepared catalysts were characterized by N_2-physisorption, XRD, H_2-TPR, H_2-chemisorption, XPS and IR spectroscopy (DRIFTS *in situ*) in order to examine the effect of structural and morphological properties on the catalytic activity and stability. Aiming to verify and classify the carbonaceous compounds on the surface of the catalysts, TPO, TGA and Raman spectroscopy were conducted with the used catalysts.

2. Experimental

2.1. Catalyst preparation

TiO_2 (P-25, Sigma–Aldrich) and Al_2O_3 (Sba200, Sasol) supports were calcined at 500 °C for 3 h. All the catalysts were prepared by incipient wetness impregnation technique using acetylacetone (Merck, 99%), palladium chloride (Aldrich, 99%) and palladium nitrate (Merck, 99%) as precursors. The amount of Pd introduced to the samples was 1 wt. %. After impregnation, the catalysts were dried at 120 °C for 15 h and calcined at 500 °C (10 °C/min) for 3 h.

All catalysts, prior to characterization, were reduced at 500 °C under H_2 flow (30 mL/min) for 2 h and then heated to 800 °C under He flow (30 mL/min) for 30 min. After this, the samples were cooled to room temperature and then passivated at liquid nitrogen temperature under a 1% O_2/He flow. The Aca, Cl and Nit terminations were used to denote Pd/Al_2O_3 and Pd/TiO_2 catalysts prepared by palladium acetylacetonate, chloride and nitrate, respectively.

2.2. Catalyst characterization

2.2.1. X-ray diffraction

X-ray diffraction measurements of passivated catalysts were carried out in a Rigaku Miniflex diffractrometer using a CuKα (1.540 Å) as the incident X-ray source with a scan rate of 0.05°/min in the range of $10 < 2\theta < 80°$.

2.2.2. BET surface area

BET surface area, pore volume and pore diameter distribution were measured with an ASAP 2020 Micromeritics analyser, employing nitrogen physisorption at −196 °C. The surface area of the reduced catalysts was estimated using the Brunauer–Emmett–Teller (BET) technique and pore volume and pore diameter distribution were calculated from the N_2 desorption curve using the Barrett–Joyner–Halenda (BJH) method. The weight of the samples was around 1 g, for all catalysts and the samples were previously dried under vacuum at 150 °C.

2.2.3. H_2-temperature programmed reduction

H_2-temperature programmed reduction of calcined catalysts were performed in an U-shaped tubular quartz reactor coupled to a mass spectrometer (*Pfeiffer Prisma*). The samples (500 mg) were dried at 250 °C for 30 min in a He flow of 30 mL/min before TPR analysis. After cooling to room temperature, TPR was conducted using a mixture of 5% H_2/Ar (30 mL/min) flowing through the sample and the temperature was raised at a heating rate of 10 °C/min up to 1000 °C.

2.2.4. H_2-chemisorption

H_2-chemisorption uptakes were measured in a Micromeritics ASAP 2010C automated gas sorption analyser. The pre-treatment of the samples (500 mg) consisted of drying in He at 150 °C for 30 min. Then, the samples were evacuated at 150 °C during 60 min followed by reduction with H_2 at 500 °C for 2 h. After that, the samples were evacuated for 60 min at the reduction temperature to remove any residual H_2, before cooling in vacuum to 100 °C for analysis [23]. The chemisorption analysis were carried out at 100 °C to avoid the formation of palladium hydride that is generally formed at room temperature and decomposes around 60–80 °C. Pd dispersion was calculated using the total chemisorption uptakes.

2.2.5. X-ray photoelectron spectroscopy

X-ray photoelectron spectroscopy of passivated catalysts was carried out using an ESCALAB 250Xi Thermo Scientific equipment with monochromatic Al Kα X-ray (1486.6 eV) with a pressure of approximately 1×10^{-9} mbar. The samples were mounted on a sample holder by means of a double-sided adhesive copper tape. The analyser was operated using an energy step size of 0.05 eV and a pass energy of 25.0 eV. The Flood Gun was used to neutralize charge build up on the surface of the samples. All spectra were calibrated using the C1s peak at 284.6 eV and Ar+- etching was used to attempt to break of oxygen film created during the passivation.

2.2.6. Acetic acid and CO DRIFTS

Diffuse reflectance infrared with Fourier transform spectroscopy was used to examine the nature of the adsorbed species on the catalysts. The system consisted in a FT-IR spectrometer (Bruker, Vertex 70) equipped with a diffuse reflectance cell with Praying Mantis geometry and a reaction chamber with ZnSe windows (Harrick, HVC-DRP-4). All spectra were obtained after average of 350 scans and a resolution of 4 cm^{-1}.

The adsorption of acetic acid was carried out at room temperature using an acetic acid/He mixture which was obtained by passing He flow (30 mL/min) in a saturator containing acetic acid maintained at 42 °C. Before the spectrum was acquired, the passivated catalysts were dried at 250 °C for 30 min with He flow (30 mL/min), reduced under H_2 flow (30 mL/min) at 400 °C (10 °C/min) for 2 h to eliminate the oxide layer formed during the passivation step, cooled under He flow until 30 °C and at this temperature, a background interferogram was collected. After adsorption of acetic acid, the catalyst was purged under flowing helium (30 mL/min) and then a new interferogram was taken at 30 °C and related to the background reference to obtain the spectrum of adsorbed acetic acid.

The acetic acid decomposition surface reaction was also followed by DRIFTS from 30 °C to 400 °C. The pretreatment of the samples was identical to that describe above. During the cooling step under He flow, the backgrounds were taken at 400, 300, 200,100 and 30 °C. Then, under acetic acid/He mixture (30 mL/min) the interferograms were taken at 30, 100, 200, 300 and 400 °C and related to the background reference (at same temperature) to obtain the spectrum of adsorbed acetic acid. The cell was kept at each temperature for 15 min.

Infrared spectroscopy of adsorbed carbon monoxide was also measured and the pretreatment was similar to that used in acetic acid DRIFTS analysis. After drying, reduction and purging of the samples, a background was taken and then 5% CO/He (30 mL/min) flow was admitted into the cell during 30 min. The samples were purged with He (30 mL/min) and under He flow the interferograms were obtained at room temperature.

2.2.7. Catalytic activity tests

Decomposition of acetic acid was performed in a quartz reactor at atmospheric pressure using 100 mg of catalyst. The reaction was carried out between 300 up to 800 °C under 100 mL/min of a 5% of CH_3COOH (Sigma–Aldrich—maintained at 42 °C) and 95% of He mixture with each temperature being kept for 50 min on stream. Acetic acid was fed to the reactor by bubbling He through a saturator containing this acid at 42 °C. The effluent gases were analyzed by a gas chromatograph (Varian CP 3800) equipped with a thermal conductivity detector and two capillary columns (Carboxen 1010 plot and CP-PoraBond Q). Prior to the reaction, the catalysts were dried and reduced for 2 h at 500 °C with pure H_2 (30 mL/min). Then, the samples were submitted to He flow (30 mL/min) and heated to 800 °C at a rate of 10 °C/min and remained at this temperature for 15 min. The reaction temperature was varied from 300 to 800 °C, with each temperature being kept for 50 min on stream. The flow rate of the gases was controlled using Brooks Instruments' mass flow controllers. The total inlet flow rate was 100 mL/min, consisting of 5% acetic acid and 95% helium. The decomposition reaction was also investigated under isothermal condition at 700 °C for 12 h in order to observe catalyst deactivation.

To verify the absence of mass transfer effects, the Weisz–Prater criterion was calculated for all the catalysts used in the acetic acid decomposition [28]. The values obtained for Weisz–Prater criterion were below 0.3. Therefore, the results reveal the absence of all transport limitations and guarantees that internal diffusion resistance did not affect the reaction. Mole fraction (y_j), conversion of acetic acid ($X_{C_2H_4O_2}$) and selectivity of hydrogen (S_{H_2}) were calculated using the following expressions:

$$y_j = \frac{n_j}{\sum n_{\text{total}}}$$

$$X_{C_2H_4O_2} = \frac{y_{CO} + y_{CH_4} + y_{CO_2} + 2y_{C_2H_4O}}{2y_{C_2H_4O_2} + y_{CO} + y_{CH_4} + y_{CO_2} + 2y_{C_2H_4O}} \times 100$$

$$S_{H_2} = \frac{y_{H_2}}{y_{H_2} + 2y_{CH_4} + y_{H_2O} + 2y_{C_2H_4O}} \times 100$$

2.2.8. Temperature programmed oxidation (TPO), thermogravimetry and mass spectroscopy (TG–MS)

Temperature programmed oxidation (TPO) experiments of used sample were performed using a thermo-gravimetric analyzer (Shimadzu DTG-60H) coupled to a quadrupole mass spectrometer (HPR-20, Hiden). The samples were weighed and dried at 200 °C (10 °C/min) with a He flow (30 mL/min) during 30 min, followed by cooling to room temperature. Then, the samples were weighed again and the temperature was increased until 900 °C (10 °C/min) with 5% O_2/He continuous flow (50 mL/min). The CO_2 produced by the oxidation of deposited carbon species was monitored by mass spectroscopy.

2.2.9. Raman spectroscopy

Raman spectra were taken in a Confocal Raman Microscope alpha 300, with Witec software, using a 50× objective lens and green laser with 532 nm wavelength. The integration time was 1.0 s and the number of scans was 400.

3. Results and discussion

3.1. Catalyst characterization

Fig. 1 shows the XRD results for passivated catalysts. The diffractograms of titania supported catalysts shows characteristic peaks of TiO_2 with anatase phase with a low part of rutile phase [29]. Typical diffraction peaks of γ-Al_2O_3 were observed for alumina supported catalysts. There was not any metallic palladium or any diffraction line of their oxides probably be due to the low palladium content.

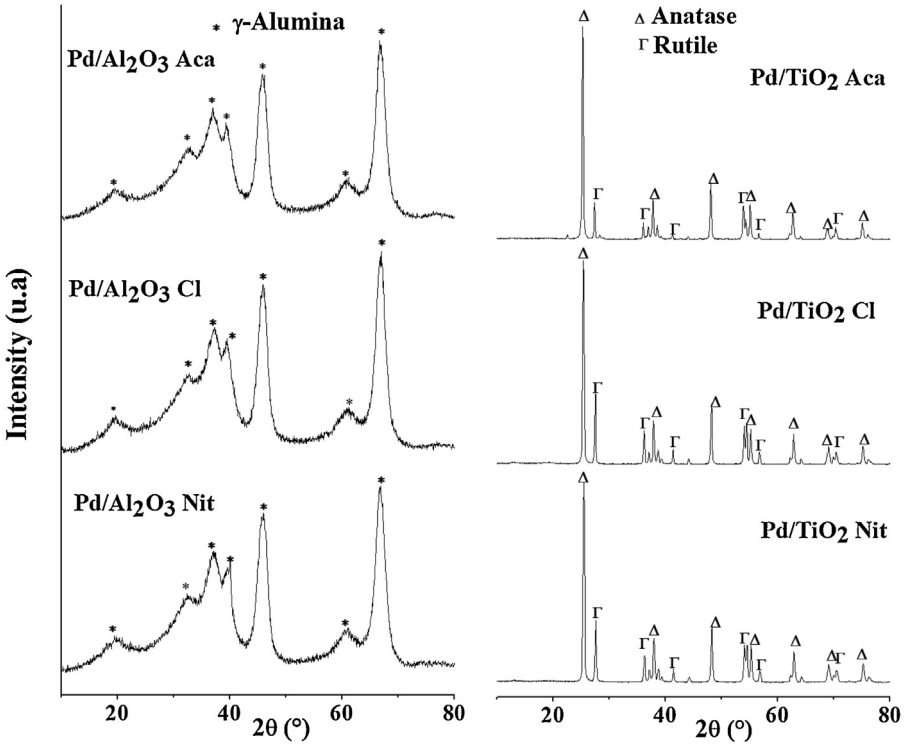

Fig. 1. XRD patterns of passivated catalysts.

Table 1
BET surface area (S_{BET}), pore size, pore volume and H/Pd ratio uptakes obtained for several catalysts.

Catalyst	Pd/Al_2O_3 Aca	Pd/Al_2O_3 Cl	Pd/Al_2O_3 Nit	Pd/TiO_2 Aca	Pd/TiO_2 Cl	Pd/TiO_2 Nit
S_{BET} (m^2/g)	172	180	193	4.5	18.1	23
Pore size (Å)	87	93	79	170	222	191
Pore volume (cm^3/g)	0.46	0.47	0.47	0.014	0.10	0.11
H/Pd (%)	16	25	16	3	2	3

BET surface area, pore volume, pore size and H/Pd ratio obtained for the several catalysts are listed in Table 1. Alumina supported catalysts exhibited higher surface area than titania supported catalysts. Pd/Al_2O_3 Nit presented the highest surface area of all catalysts (193 m^2/g), with a pore volume of 0.47 cm^3/g. BET surface areas of the catalysts with same support were similar, except for Pd/TiO_2 Aca whose surface area was 4.5 m^2/g because during the treatment at 800 °C some pores collapsed and as consequence, the surface area decreased. Also, at high temperature the anatase phase is converted into the more stable rutile (Fig. 1) and unfortunately, this phase transition to rutile is associated with a significant loss in surface area [30].

Fig. 2 shows the adsorption isotherms of Pd/Al_2O_3 Aca, Pd/Al_2O_3 Cl and Pd/Al_2O_3 Nit catalysts were type IV isotherms. The isotherms showed a clear H2 type hysteresis, which indicates 'ink bottle' type pores. Pd/TiO_2 Aca, Pd/TiO_2 Cl and Pd/TiO_2 Nit catalysts presented type III isotherms with H3 type hysteresis which represents 'slit-like' pores [31].

Titania supported catalysts, showed very low H/Pd values, when compared with alumina supported catalysts. Titania is a partially reducible support and high temperature reduction (500 °C), leads to partially reduced species (TiO_2-x) which can easily migrate over metal particles, causing low capacities of hydrogen adsorption. This phenomenon is called SMSI effect (strong metal-support interaction) [32,33]. On the other hand, for alumina supported catalysts, pre-treatment at 800 °C that could cause sintering of active phase. Sintering is usually significant when material is heated above its Tamman temperature ~650 °C for Pd [34]. However, among all alumina supported catalysts, the Pd/Al_2O_3 Cl showed the highest dispersion (25%). Some authors [21,35] affirm that chlorides interact with the hydroxyl groups of supports and favor the dispersion of the metallic phase.

H_2-TPR profiles of the calcined catalysts are shown in Fig. 3. All the catalysts exhibited a peak at room temperature, ascribed to the reduction of palladium oxide (PdO) to metallic palladium (Pd^0).

Besides the reduction of PdO, hydrogen absorption in the reduced palladium and adsorption on the metallic surface are also responsible for the hydrogen consumption at room temperature [36]. This fact was taken in account when the hydrogen consumption at room temperature was calculated. For all supported catalysts, the results showed negative TPR peaks in the range of 60–80 °C which are attributed to Pd hydride (β-PdH_2) decomposition, formed at room temperature from the absorption of hydrogen within the structure of metallic Pd [32,36,37]. Generally, larger particles (>2 nm) have higher storage capacity than the smaller ones to form hydrides. The decomposition of palladium hydrides takes place at higher temperatures in the case of small palladium particles [38]. Alumina supported catalysts exhibited a peak at ~355 °C possible due to the reduction of small particles of PdO, which interact most strongly with the support. Similar results have been reported with different types of interaction between palladium and the support [38–41]. For supported palladium catalysts prepared with palladium chloride, the peak may also include the hydrogen consumption due to PdO_xCl_y reduction. These species are

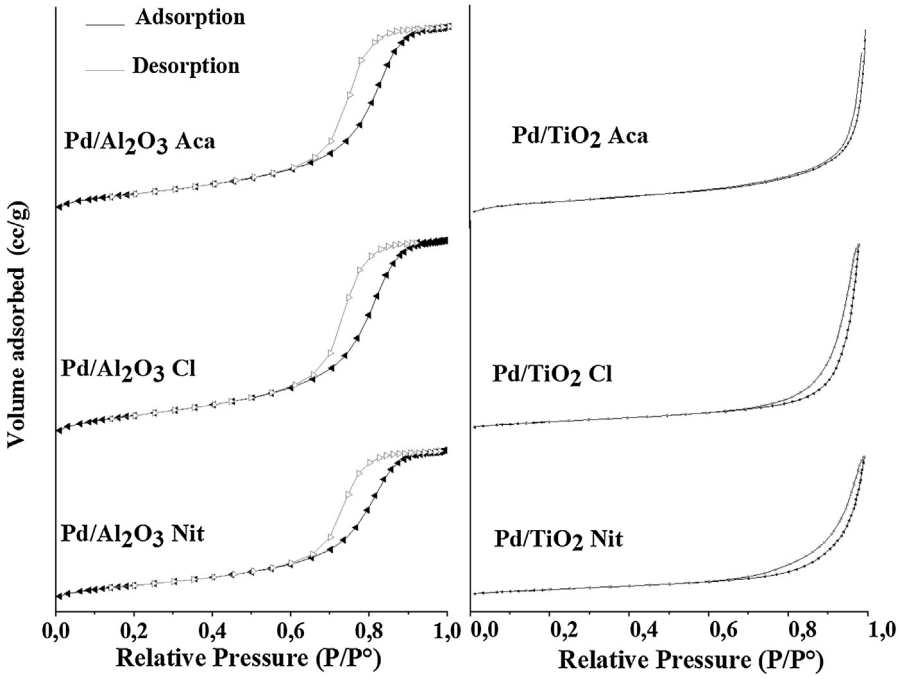

Fig. 2. N_2 adsorption–desorption isotherms for palladium-supported catalysts.

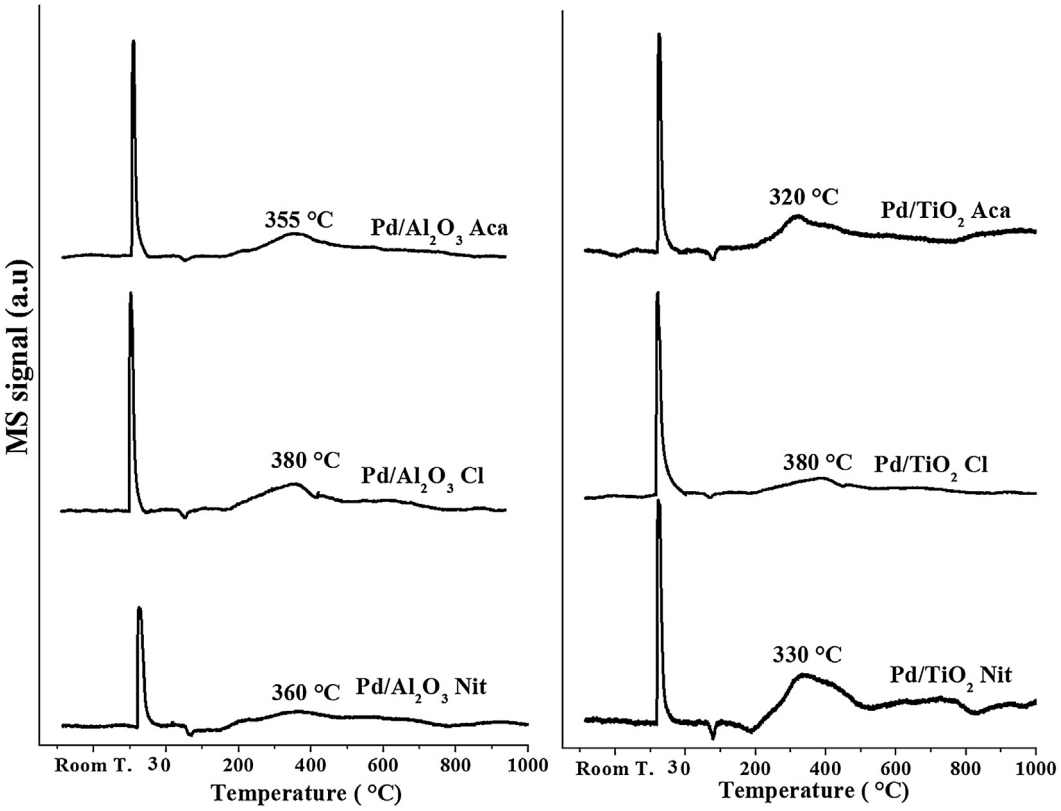

Fig. 3. TPR profiles of the investigated catalysts.

formed during the calcination step on catalysts prepared with $PdCl_2$ as palladium precursor [42]. In the case of titania supported catalysts the high temperature peaks are attributed to the reduction of titania to form partially reduced species, TiO_x [43]. This fact is consistent with H_2-chemisorption results, in which titania supported catalysts presented low H/Pd ratios attributed to a decoration of metallic particles by partially reduced species. Hydrogen consumption during palladium oxide reduction is shown in Table 2.

Pd/Al_2O_3 Nit presented the higher H_2-consumption at room temperature among all alumina supported catalysts and as mentioned earlier, for alumina supported catalysts, the hydrogen consumption at high temperatures was assigned to PdO species

Table 2
H_2 consumption during temperature programmed reduction at room temperature and at high temperatures and degree of reduction.

Catalysts	Room temperature H_2 consumption (μmol H_2/g_{cat})	High temperatures H_2 consumption (μmol H_2/g_{cat})	Degree of reduction (%)
Pd/Al_2O_3 Aca	28.8	77.9	98.7
Pd/Al_2O_3 Cl	44.4	68.8	100
Pd/Al_2O_3 Nit	56.0	53.3	100
Pd/TiO_2 Aca	21.3	–	43.4
Pd/TiO_2 Cl	102.1	–	94.5
Pd/TiO_2 Nit	41.1	–	55.4

more strongly bonded with the support. Hydrogen uptakes found for alumina supported catalysts were near the stoichiometric amount necessary for the reduction of PdO which was reflected in degree of reduction indicating that at temperatures above 450 °C all palladium was reduced. On the other hand, except for Pd/TiO_2 Cl, all the titania supported catalyst showed lower hydrogen consumption and consequently low degree of reduction at room temperature when compared with alumina supported catalysts. TPR results indicated the reduction at 500 °C under hydrogen flow is sufficient to totally reduce Pd in the examined catalysts.

The passivated catalysts have also been characterized by XPS and the results for Pd 3d region are shown in Fig. 4 and Table 3. The data indicated both Pd^{2+} and Pd^0 species exist in all the catalysts. The binding energies at 335.2 eV and 340.4 eV corresponds to Pd^0 $3d_{5/2}$ and Pd^0 $3d_{3/2}$, respectively while the binding energies at 336.2 eV and 341.4 eV corresponds to Pd^{2+} $3d_{5/2}$ and Pd^{2+} $3d_{3/2}$, respectively [23,44].

The peak areas of metallic phases are higher than oxide phases indicating that reduction and passivation steps were efficient. The existence of Pd^{2+} species is due to the palladium oxide shell formed during the passivation step. The XPS spectra of Pd/Al_2O_3 Cl displayed an additional small peak at 337.3 eV which is attributed to the $PdCl_2$ species from palladium precursor [44]. Pd/support ratios for the alumina supported catalysts were higher than the ratios obtained for titania supported catalysts which indicated that alumina supported catalysts had more palladium on their surfaces.

SMSI was also identified for the titania supported catalysts because significant binding energy (BE) shift was observed for O1s and Ti2p (not shown). The negative shift of Ti $2p_{3/2}$ indicated that titania is partially reduced into Ti^{3+} and oxygen vacancies were formed [30,45]. When oxygen vacancies are formed at metal-support interface of titania supported catalysts, oxygen from the gas phase could be dissociatively adsorbed and the other being coordinated to the five-coordinated Ti^{4+} sites. The O1s BE region is rather complex because it contains contribution not only from several oxygen species (such TiO_2, PdO and hydroxyl groups) but also from Pd. The O1s BE of passivated titania is slightly lower and a significant shoulder peaks at approximately 532 eV, corresponding to the chemisorbed oxygen were also observed [30,45]. These results clearly indicated the existence of an SMSI effect and this behavior is in agreement with H_2-chemisorption results and confirms the presence and the influence of the decoration effect in the case of titania supported catalysts, causing a low exposure of the active phase.

Infrared spectroscopy of adsorbed CO for all the catalysts is shown in Fig. 5. In the case of palladium catalysts, two major peaks are commonly attributed to linearly-bonded CO (above 2000 cm^{-1}) and bridged-bonded CO (below 2000 cm^{-1}) [21]. The difference in the position of CO absorption frequencies demonstrates that the nature of Pd precursors plays a role on the Pd sites properties. Also, the precursor–support interaction influences the Pd particle size distribution, which determines the nature of sites available on the surface.

CO adsorption bands on titania catalysts were not well defined, however they can be assigned to linearly-bonded CO [46] (2045 cm^{-1}) and bridged-bonded CO (1905 cm^{-1}) for Pd/TiO_2 Aca catalyst. Titania is a reducible support and it is able to decorate palladium atoms and hinder CO adsorption. This finding is explained by SMSI effect, which was detected in H_2-TPR, H_2-chemisorption and XPS. For alumina supported catalysts, there were two bands around 1905 cm^{-1} and 2045 cm^{-1}, typical of CO adsorbed on metallic palladium. These bands can be assigned to bridge-bonded and linear bonded adsorbed CO, respectively. The Pd/Al_2O_3 Aca catalyst showed only one band at 1905 cm^{-1} for bridged-bonded CO, while Pd/Al_2O_3 Cl and Pd/Al_2O_3 Nit catalysts exhibited two bands due to bridged-bonded CO (Pd/Al_2O_3 Cl (1905 cm^{-1} and 1970 cm^{-1})) and Pd/Al_2O_3 Nit (1910 cm^{-1} and 1970 cm^{-1}). The intensity of bridge-bonded bands were higher than linear bonded, which was a consequence of the level of dispersion [47] observed for alumina supported catalysts. Binding of carbon monoxide to metal surfaces occurs *via* a 5σ donation of the highest occupied molecular orbital (HOMO) to the metal surface and $2\pi^*$ back-donation from the metal surface to the lowest unoccupied molecular orbital (LUMO) [48]. Bridged-bonded CO bands differ in position depending on several factors such as coordination of metal atoms, geometry of adsorption sites and surface coverage degree. On supported palladium catalysts, bridged-bonded CO located at higher frequencies may be ascribed to CO adsorption on Pd(100) surfaces and the bands located at lower frequencies are associated to CO adsorption on Pd(111) surfaces [49]. Therefore, Pd/Al_2O_3 Cl and Pd/Al_2O_3 Nit catalysts contain both Pd(100) and Pd(111) orientation surface sites, while CO absorption at lower frequencies for Pd/Al_2O_3 Aca suggest the presence of surface sites with Pd(111) orientation. This behavior is in agreement with Monteiro et al. [21] who studied the effect of palladium precursor on the oxidation of carbon monoxide over Pd/Al_2O_3 and $Pd/CeO_2/Al_2O_3$ catalysts.

Fig. 6 shows infrared spectra after adsorption of acetic acid at room temperature on alumina and titania supported catalysts. All the catalysts exhibited molecular adsorption of acetic acid. The band attributed to weakly chemisorbed molecular acetic acid interacting with surface hydroxyl groups can be assigned to carbonyl stretching ν(C=O). Undissociated acetic acid forms monomers and dimers in both phases, liquid and gas, at approximately 1782–1790 cm^{-1} and 1175 cm^{-1}, respectively [50]. At room temperature, the bands around 1724 cm^{-1} and 1294 cm^{-1} were assigned to some vibrations of dimers of acetic acid. For Pd/Al_2O_3 Aca this molecular adsorption is characterized by a band at 1722 cm^{-1} for ν(C=O), 1372 cm^{-1} for ν(C—O), 1294 cm^{-1} for ν(C-C), 1072 cm^{-1} for ρ(CH_3) and 960 cm^{-1} for γ(O—H) [46]. Similar bands were detected for the other catalysts as shown in Fig. 6 and Table 4.

For Pd/Al_2O_3 Aca and Pd/Al_2O_3 Cl catalysts, the surface acetate species were characterized by a band at 1540 cm^{-1} for antisymmetric carboxylate (ν_{as}(COO)) and a band at 1426 cm^{-1} for symmetric carboxylate (ν_s(COO)). The splitting of carboxylate stretching frequencies determines the configuration of acetate species as monodentate, chelating bidentate or bridging bidentate configuration [46]. In monodentate configuration, the splitting between the symmetric ν_s(COO) and anti-symmetric ν_a(COO) bands is greater than 160 cm^{-1} and the acetate is bound to the surface through only

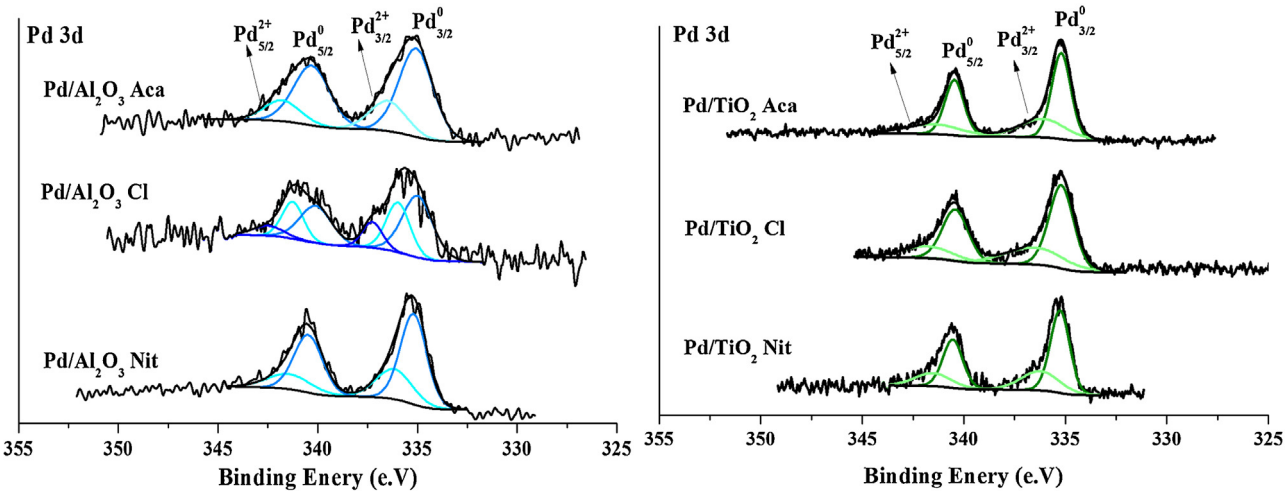

Fig. 4. XPS spectra of the passivated catalysts in the Pd 3d region.

Table 3
Binding energies of Pd $3d_{5/2}$ and Pd $3d_{3/2}$ peaks of the different samples.

Catalyst	Binding energy (eV)				Pd/support
	Pd^0 $3d_{5/2}$	Pd^0 $3d_{3/2}$	Pd^{2+} $3d_{5/2}$	Pd^{2+} $3d_{3/2}$	
Pd/Al_2O_3Aca	335.0	340.3	336.3	341.7	0.027
Pd/Al_2O_3Cl	335.0	340.1	335.9	341.2	0.018
Pd/Al_2O_3Nit	335.2	340.4	336.2	341.4	0.059
Pd/TiO_2Aca	335.2	340.4	336.1	340.4	0.018
Pd/TiO_2Cl	335.2	340.4	336.5	341.8	0.023
Pd/TiO_2Nit	335.2	340.5	336.2	341.5	0.010

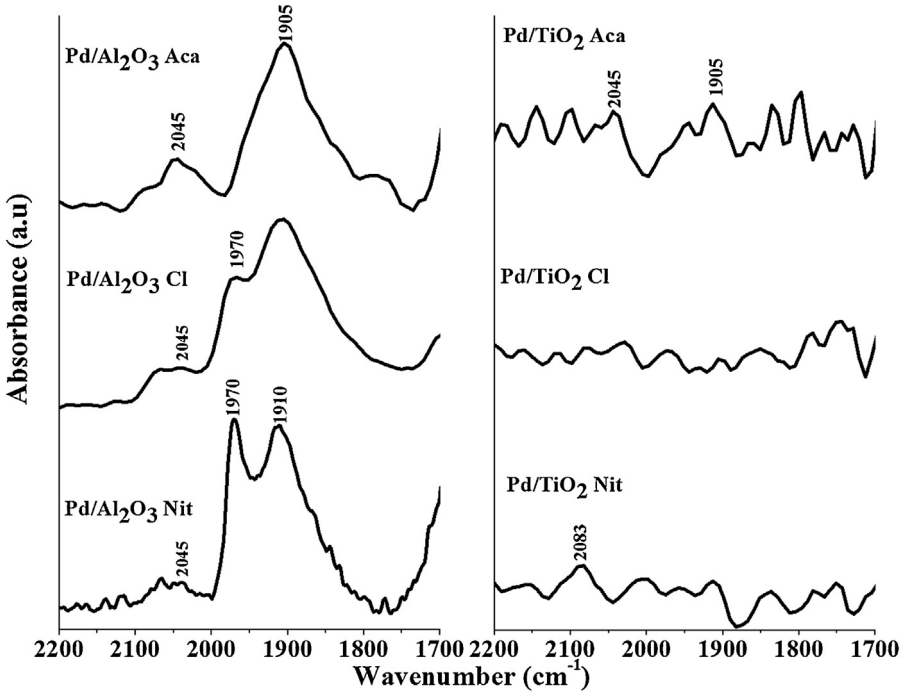

Fig. 5. Infrared spectra of CO adsorption for all Pd/Al_2O_3 and Pd/TiO_2 catalysts.

of its oxygen atoms. In the case of the chelating bidentate mode, the splitting is considerably lower than ~160 cm^{-1}, with the acetate bounded to one surface metal cation through both of its oxygen atoms. The bridging configuration is characterized by a splitting larger than of the chelating bidentate, but it is similar to the ionic value and acetate is bound to the surface with two oxygen atoms bound to two metal sites [46]. For Pd/Al_2O_3 Aca and Pd/Al_2O_3 Cl catalysts, the splitting was 114 cm^{-1} that suggest a chelating bidentate configuration. The Pd/Al_2O_3 Nit catalyst exhibited a band characteristic of molecular acetic acid at 1722 cm^{-1} and there was only a band characteristic of acetate species at 1426 cm^{-1} (ν_s(COO)). The band at 1600 cm^{-1} was assigned to the O—C=O stretch and

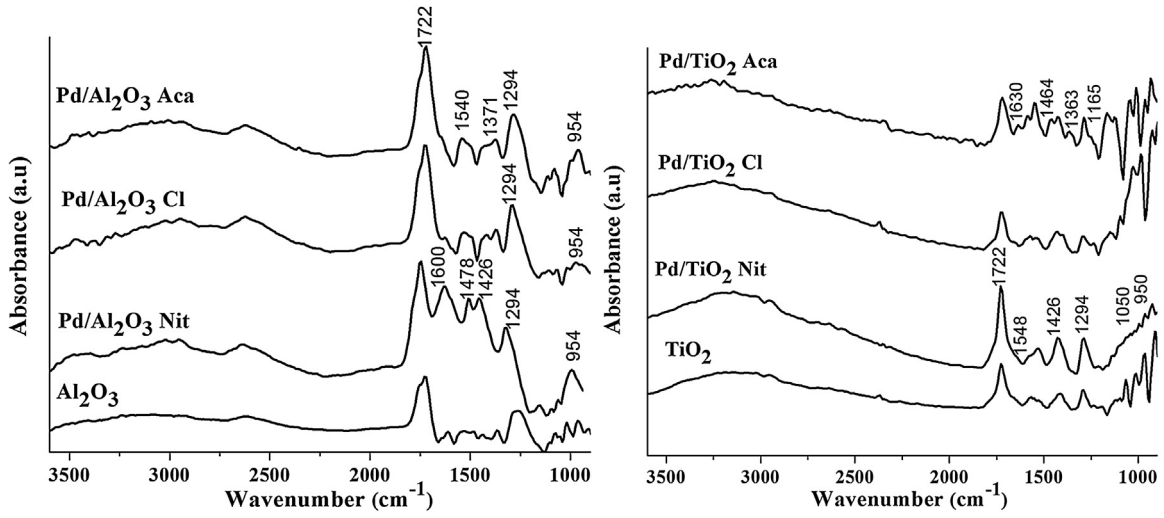

Fig. 6. DRIFT spectra of surface species formed following adsorption of acetic acid on alumina (left) and titania (right) palladium supported catalysts.

Table 4
Vibrational mode assignments for surface species formed by acetic acid adsorption at room temperature on palladium catalysts.

Band	Infrared band wavenumber (cm^{-1})							
	Pd/Al_2O_3 Aca	Pd/Al_2O_3 Cl	Pd/Al_2O_3 Nit	Pd/TiO_2 Aca	Pd/TiO_2 Cl	Pd/TiO_2 Nit	Al_2O_3	TiO_2
$\nu(C{=}O)_{HOAc}$	1722	1722	1722	1726	1726	1726	1722	1727
$\nu(C{-}O)_{HOAc}$	1372	1371	–	1363	–	–	1372	–
$\nu(-C)_{HOAc}$	1294	1294	1294	1294	1294	1294	1294	1294
$\gamma(O{-}H)_{HOAc}$	960	960	960	963	–	962	960	960
$\rho(CH_3)$	1072	1070	1062	1050	–	1050	–	–
$\nu_{as}(COO)_{acetate}$	1540	1540	–	1548	1566	1573	–	–
$\nu_s(COO)_{acetate}$	1426	1426	1426	1466	1427	1426	–	k

corresponded to a monodentate acetate species [51]. In the case of the spectra for alumina supported catalysts, the bands for acetate species were of low intensity and mainly demonstrated the adsorption of molecular acetic acid.

Molecular adsorption of acetic acid and acetate species were formed on the titania supported catalysts, as identical bands were observed during acetic acid adsorption on alumina supported catalysts, but with minor intensity as shown in Fig. 6 and Table 4. This behavior indicates a lower adsorption of acetic acid and lower affinity of acetic acid with titania possibly due to the high particle coverage of palladium by the partially reduced species of the support. The same bands that were observed for the titania catalysts were also observed for pure TiO_2. This may indicate that palladium is less accessible on the surface of catalysts for the adsorption of acetic acid and its dissociated species.

Alumina supported catalysts exhibited both acetic acid and CO adsorption possible due to the availability palladium on catalysts surfaces. However, titania supported catalysts showed lower acetic acid adsorption and scarce CO adsorption. The above-mentioned results indicate that on all catalysts, the acetic acid was adsorbed mainly through the acetate species.

Fig. 7 shows infrared spectra after adsorption of acetic acid on several catalysts at room temperature, 100, 200, 300 and 400 °C. At room temperature, both molecular acetic acid and acetate species were formed, as identical bands were observed earlier.

For Pd/Al_2O_3 Aca catalysts, at 100 °C, a band at 1489 cm^{-1} was assigned to bridging bidentate acetate species, the most stable configuration and it decomposes with further heating [52]. The molecular adsorption of acetic acid decreases with the temperature increase indicating that molecular acetic acid is weakly bounded. The bands at 1789 cm^{-1} and 1682 cm^{-1} are indicative of acetic acid monomer and acyl species (ν(C=O)), respectively [50]. Acetate species at 1426 cm^{-1} (symmetric carboxylate (ν_s(COO))), disappears almost completely upon heating from 300 °C up to 400 °C, while the band at 1545 cm^{-1}(antisymmetric carboxylate (ν_{as}(COO))) decreased its intensity with temperature increased. At 300–400 °C, bands at 2306 cm^{-1} (CO_2 ν(CO)) and 1642 cm^{-1} (δ(OH) water) were also detected, which suggests that CO_2 and H_2O can result from acetate species decomposition (bidentate acetate, bridging acetate and acyl species) [53]. Similar bands were detected for Pd/Al_2O_3 Cl catalyst with some differences in intensity and position of the characteristic bands. For Pd/Al_2O_3 Nit the intensity of molecular acetic acid band also decreased when the temperature was elevated. At 200 °C, there was no evidence of molecular acetic acid as in previous results. With temperature increase, bands at 1790 cm^{-1} (monomeric acetic acid), 1680 cm^{-1} (acyl species) and 2372 cm^{-1} (CO_2) were detected. Disappearance of the bands assigned to molecular acetic acid, mainly at temperatures between 300 and 400 °C, suggests that dissociated species of acetic acid are the precursors of CO_2 and H_2O.

For titania supported catalysts, at temperatures between 100 and 400 °C, molecular (~1722 cm^{-1}) and monomeric (~1790 cm^{-1}) acetic acid was detected. At 400 °C, for Pt/TiO_2 Aca and Pd/TiO_2 Nit catalysts, characteristic bands of CO_2 were observed at ~2037 cm^{-1} with the disappearance of monomeric acetic acid and intense decrease in intensity of acetate species.

3.2. Decomposition of acetic acid

The results of conversion of acetic acid during the decomposition reaction on the several catalysts are shown in Fig. 8. Alumina supported catalysts were the most active catalysts and presented almost 100% of acetic acid conversion above 600 °C. In contrast, titania supported catalysts were not significantly active

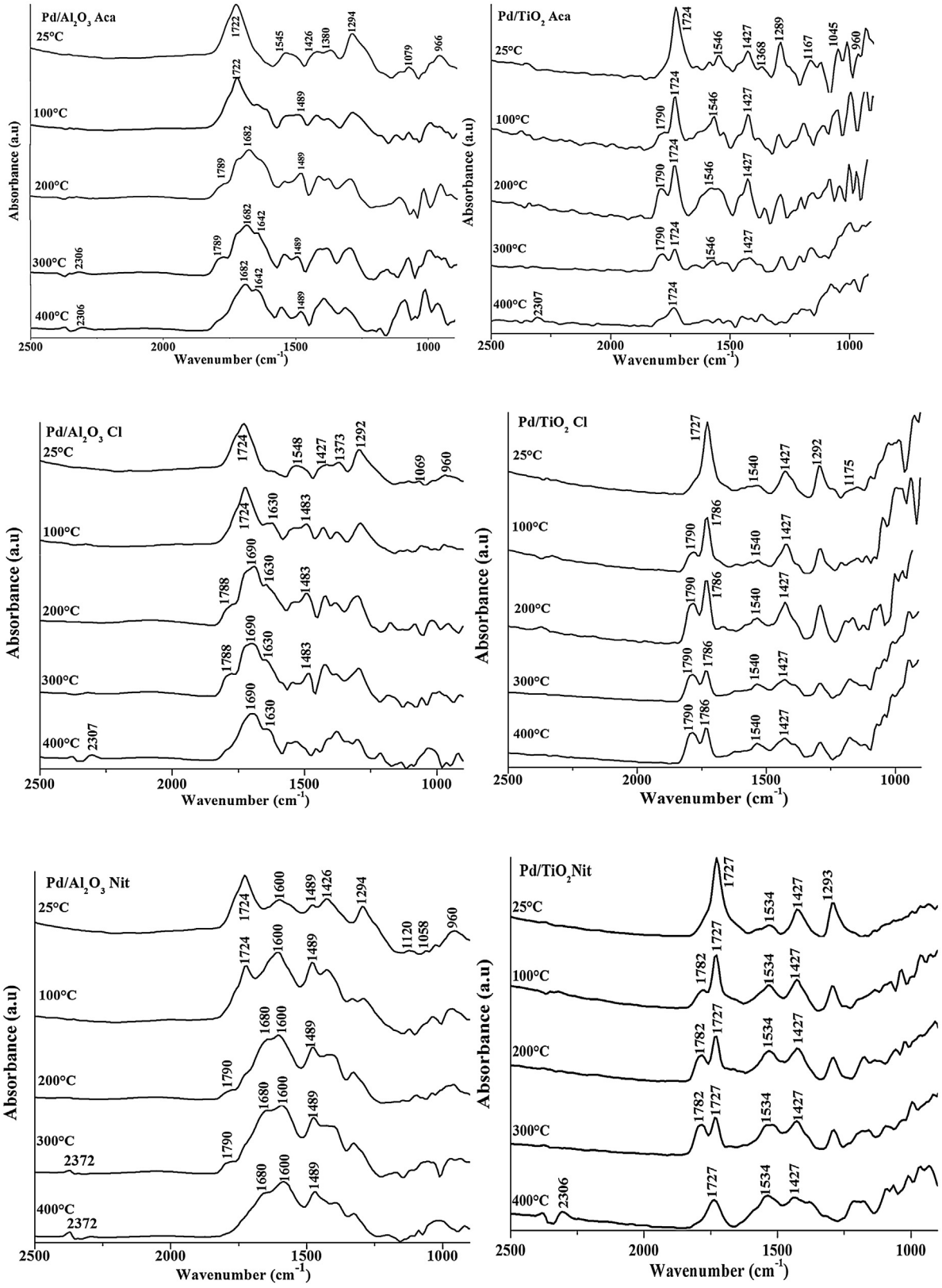

Fig. 7. DRIFT spectra of surface species formed during adsorption of acetic acid, at different temperatures on alumina and titania palladium supported catalysts.

at temperatures below 700 °C. Conversion curves indicate that higher temperature favored acetic acid conversion and the following sequence of catalytic activity was pointed out: Pd/Al_2O_3 Nit > Pd/Al_2O_3 Aca > Pd/Al_2O_3Cl> Pd/TiO_2 Aca > Pd/TiO_2 Cl > Pd/TiO_2 Nit.

Table 5 summarizes the initial rate for the acetic acid decomposition ($-r_A$), the turnover frequency (TOF) for the Pd supported

Table 5
Initial rate, TOF for acetic acid decomposition over Pd supported catalysts at 400 °C and carbon amount of carbon deposits after reaction.

Catalysts	$-r_A$(mmol/g_{cat} h)	TOF (s^{-1})	Carbon amount (g/g_{cat})
Pd/Al_2O_3Aca	9.8	0.18	0.7
Pd/Al_2O_3 Cl	4.3	0.05	0.7
Pd/Al_2O_3Nit	13.0	0.24	2.4
Pd/TiO_2 Aca	7.1	0.82	0.5
Pd/TiO_2 Cl	0.5	0.065	0.3
Pd/TiO_2 Nit	1.1	0.10	0.6

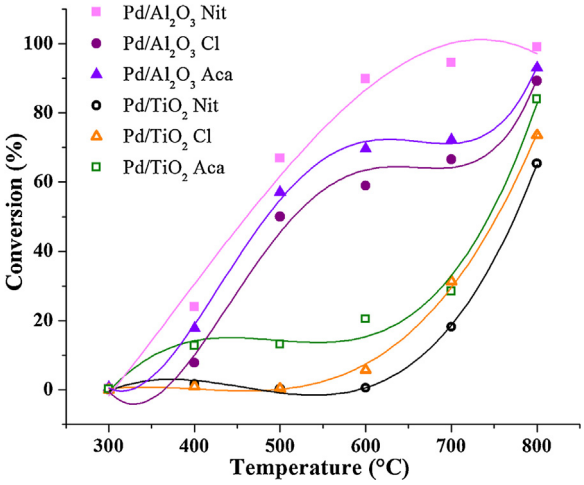

Fig. 8. Conversion of acetic acid during decomposition over palladium supported catalysts. Reaction conditions: Total flow: 100 mL/min (5% $C_2H_4O_2$; 95% He). Catalyst weight: 100 mg.

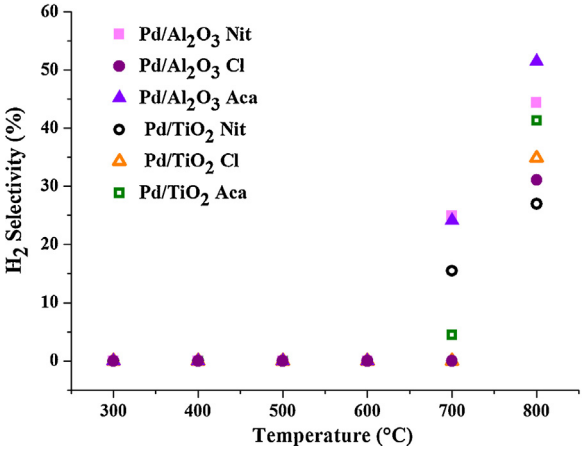

Fig. 9. Selectivity toward hydrogen production over all the catalysts during acetic acid decomposition Reaction conditions: Total flow: 100 mL/min (5% $C_2H_4O_2$; 95% He). Catalyst weight: 100 mg.

catalysts and the carbon amount present in the catalysts after decomposition of acetic acid. Turnover frequencies at 400 °C were calculated based on H_2 chemisorption as estimate of the number of active sites. The catalysts presented TOF values in the following order: Pd/TiO_2 Aca > Pd/Al_2O_3 Nit > Pd/Al_2O_3 Aca > Pd/TiO_2 Nit > Pd/TiO_2 Cl > Pd/Al_2O_3 Cl. These results suggest that catalysts prepared with acetylacetonate and nitrate were more active for acetic acid decomposition under clean conditions. Catalysts prepared with palladium chloride showed the lower TOF. Additionally, the results indicate the formation of metal-interface sites for titania supported catalysts. Fig. 9 shows the selectivity toward hydrogen production over all the catalysts. Hydrogen was only detected above 600 °C and for catalysts prepared with palladium chloride it was only detected at 800 °C. H_2 selectivity followed a similar behavior to the conversion of acetic acid. Pd/Al_2O_3 Nit and Pd/Al_2O_3 Aca were more active at higher temperatures and exhibited higher hydrogen formation. Catalysts prepared with palladium acetylacetonate as precursor were more selective to H_2 production. H_2 yield was higher at 800 °C (52%) for the Pd/Al_2O_3 Aca catalyst.

As observed by Brijaldo et al. [19], the products of acetic acid decomposition were H_2, CO, CH_4, CO_2, H_2O and acetaldehyde (C_2H_4O) and Fig. 10 shows the reactant and product distribution (molar fraction) for all the catalysts as a function of reaction temperature. For alumina supported catalysts, at 300 °C only CO_2 and H_2O were observed. Then, at 400 °C acetaldehyde (C_2H_4O) was also observed. Acetic acid decomposition could yield acetaldehyde and oxygen, but only acetaldehyde was detected because the oxygen produced quickly reacted with acetic acid to form CO_2 and H_2O. Acetaldehyde also comes from the hydrogenation of acetic acid mainly at temperatures between 500 and 600 °C. When the temperature was increased, the same behavior was observed at 500 °C and 600 °C and three additional reactions were proposed: acetic acid decomposition to CO and H_2, methanation derived from the reaction between the produced H_2 and CO_2 and a water–gas shift reaction.

At 700 °C, hydrogen detection began for Pd/Al_2O_3 Aca and Pd/Al_2O_3 Nit and there was the formation of a high amount of CO, which suggests that the decomposition of acetic acid into H_2 and CO was favored from this temperature. Other important reaction is the acetic acid reforming which was observed for all alumina supported catalysts. As can be seen in Fig. 10, when H_2 was observed at temperatures between 700 and 800 °C, the amount of water decreased while CO_2 increased. The Boudouard reaction has to be taken in account for all catalysts. The several products mentioned above can be explained by the following chemical reactions:

$$C_2H_4O_2 \rightarrow C_2H_4O + \frac{1}{2}O_2 \quad (2)$$

$$C_2H_4O_2 + 2O_2 \rightarrow 2CO_2 + 2H_2O \quad (3)$$

$$C_2H_4O_2 \rightarrow 2CO + 2H_2 \quad (4)$$

$$C_2H_4O_2 + H_2 \rightarrow C_2H_4O + H_2O \quad (5)$$

$$CO_2 + 4H_2 \rightarrow CH_4 + 2H_2O \quad (6)$$

$$CO + H_2O \leftrightarrow CO_2 + H_2 \quad (7)$$

$$C_2H_4O_2 + 2H_2O \rightarrow 2CO_2 + 4H_2 \quad (8)$$

$$2CO \rightarrow C + CO_2 \quad (9)$$

Titania supported catalysts presented a low activity for the conversion of acetic acid as observed above (Fig. 8). The same products were observed when compared with alumina supported catalysts, but with low molar fractions. At temperatures between 300 and 600 °C, water, CO_2 and some acetaldehyde were observed.

The results indicated that palladium precursor and also the support have strong influence in the catalytic behavior of the prepared catalysts. Also, the results indicate that palladium acetylacetonate is a suitable precursor of palladium catalysts for decomposition of acetic acid because it was the most selective to hydrogen. On

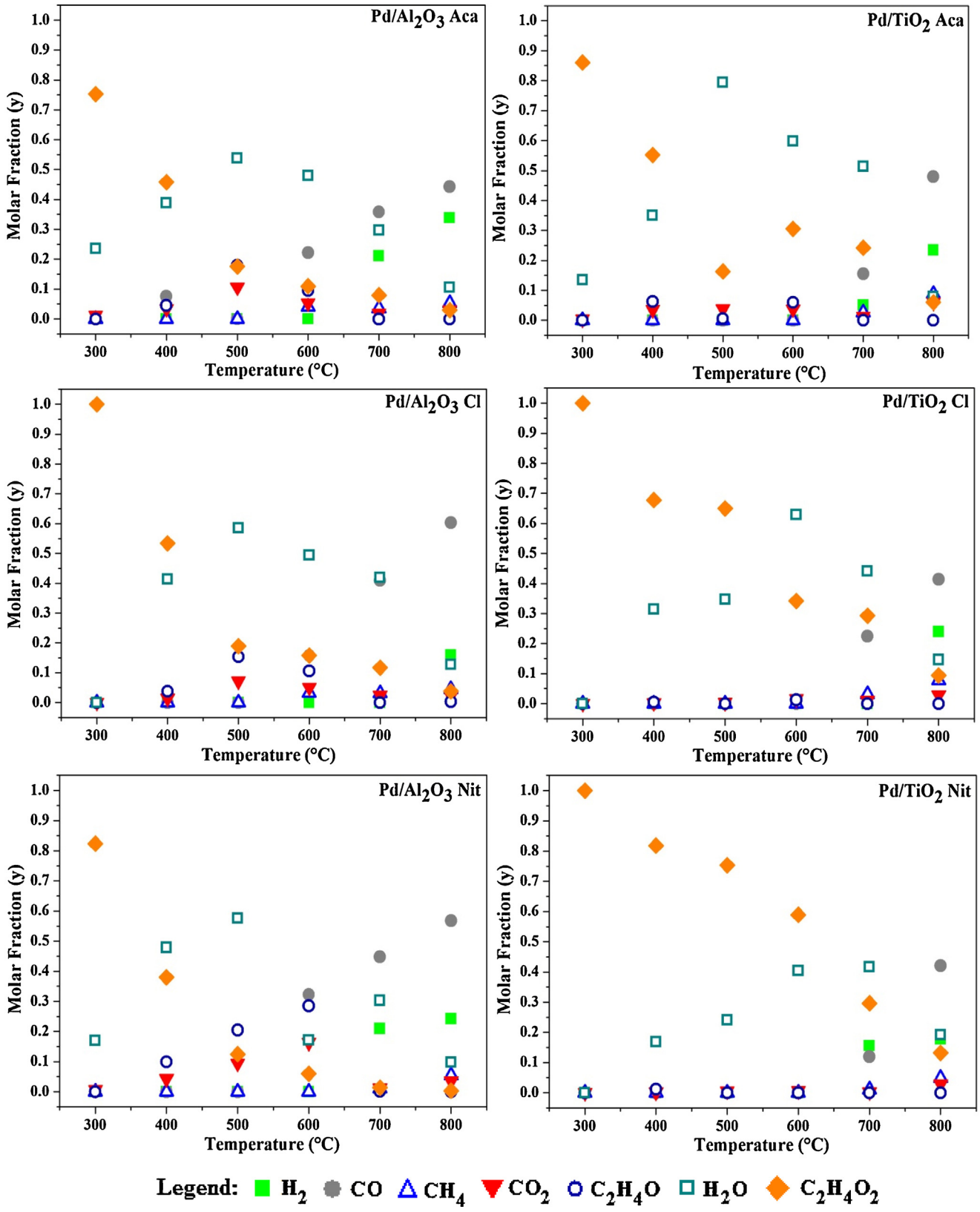

Fig. 10. Product distribution over palladium catalysts during acetic acid decomposition Reaction conditions: Total flow: 100 mL/min (5% $C_2H_4O_2$; 95% He). Catalyst weight: 100 mg.

the other hand, palladium chloride showed to be less adequate to prepare catalysts for decomposition of acetic acid, since chloride species inhibited the catalytic reaction. DRIFTS results showed that the mode of acetic acid adsorption was influenced by the support. Acetate formation was favored on alumina supported catalysts, but a molecular mode of adsorption was preferred on titania

supported catalysts. Besides, catalytic activity varied appreciably with apparent metal dispersion. Alumina supported catalysts presented higher adsorption capacity than titania supported catalysts due to SMSI effect. Taking into account our previous work [19], we suggest that hydrogen selectivity is influenced by several factors: metal site distribution, metal-support interface effect and nature of the support. In addition, the presence of dissociated acid acetic species also favors the hydrogen production from acetic acid decomposition. Although SiO_2 and Al_2O_3 are non-reducible supports, Pd/SiO_2 and Pd/Al_2O_3 presented different catalytic behaviors. Pd/SiO_2 catalyst was not able to produce H_2, while Pd/Al_2O_3 catalysts presented high hydrogen formation. This fact was due to the existence of dissociated species of acetic acid as monodentate, bidentate chelating and bridging acetates and acyl species on Pd/Al_2O_3. On the other hand, Pd/SiO_2 mainly exhibited adsorption of molecular acetic acid. Other factor that contributed to high performance of Pd/Al_2O_3 was the dispersion and orientation of active phase. Pd/Al_2O_3 catalysts showed 16–20% dispersions (Table 1) and the CO-DRIFTS results indicated a high density of corners and edges and such imperfections (Fig. 4) while Pd/SiO_2 only presented 2% dispersion and low distribution of palladium as was detected in the DRX analysis as consequence of agglomeration of active phase. The metal-support interface effect also contributes to hydrogen production. The catalysts supported on reducible oxides, like Pd/TiO_2 (this work) and Pd/Fe_2O_3, Pd/Nb_2O_5 and Pd/La_2O_3 [19] presented formation of hydrogen. They exhibited Pd^0–MO_x (MO_x: partially reduced support species), which favored the adsorption of dissociated species of acetic acid.

3.3. Stability tests

The results of stability tests under isothermal conditions (700 °C) are shown in Fig. 11. As observed, all the catalysts exhibited the same trend of stability, so the conversions decreased with the time. In the first 4–5 h alumina supported catalysts showed better stability than titania supported catalysts. Pd/Al_2O_3 Nit exhibited the best stability among all catalysts. Pd/Al_2O_3 Cl evidenced a slight increase of conversion of acetic acid in the first 3 h, but after that time the conversion decreases and remained with low conversion as consequence of catalysts deactivation. In the case of titania supported catalyst, the conversion decreased during the first 3 h and then remained low and constant. The deactivation of these catalysts is due to carbon accumulation onto the surface of palladium.

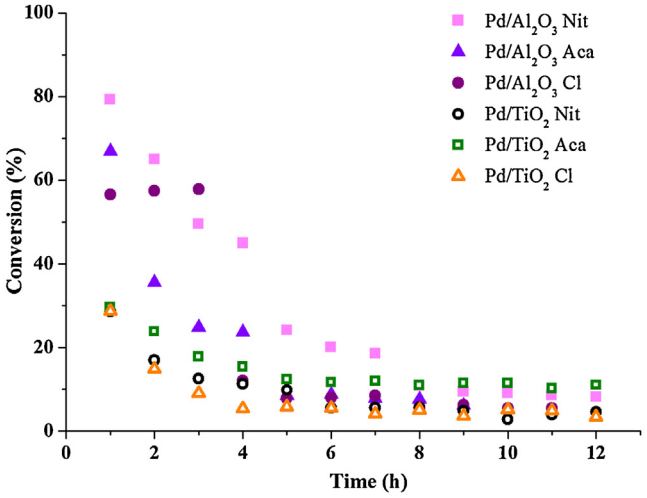

Fig. 11. Results of thermal stability tests in the acetic acid decomposition at 700 °C. Reaction conditions: Total flow: 100 mL/min (5% $C_2H_4O_2$; 95% He). Catalyst weight: 100 mg.

Raman spectroscopy and TPO experiments were useful to characterize carbon deposits on the surface of the catalysts after decomposition of acetic acid (Figs. 12 and 13). The amount of carbon deposit was defined as the mass of carbon deposited *per* mass of catalyst (Table 5). Fig. 12 shows the Raman spectra of the used catalysts recorded at room temperature. All catalysts exhibited a D band, centered at ~1344 cm^{-1} and a G band, centered at ~1586 cm^{-1} [54,55]. These results indicate that there may be two distinct carbon species on the catalyst surfaces after the acetic acid decomposition. The D band is associated to the Raman mode of C—C bond stretching due to disordered defective carbon structures and it is generally associated to an amorphous carbon or amorphous carbon hydrogenate [55] and the G band corresponds to the ordered and well graphitized carbon forms. These results indicate that the used catalysts presented a mixture of disordered and ordered

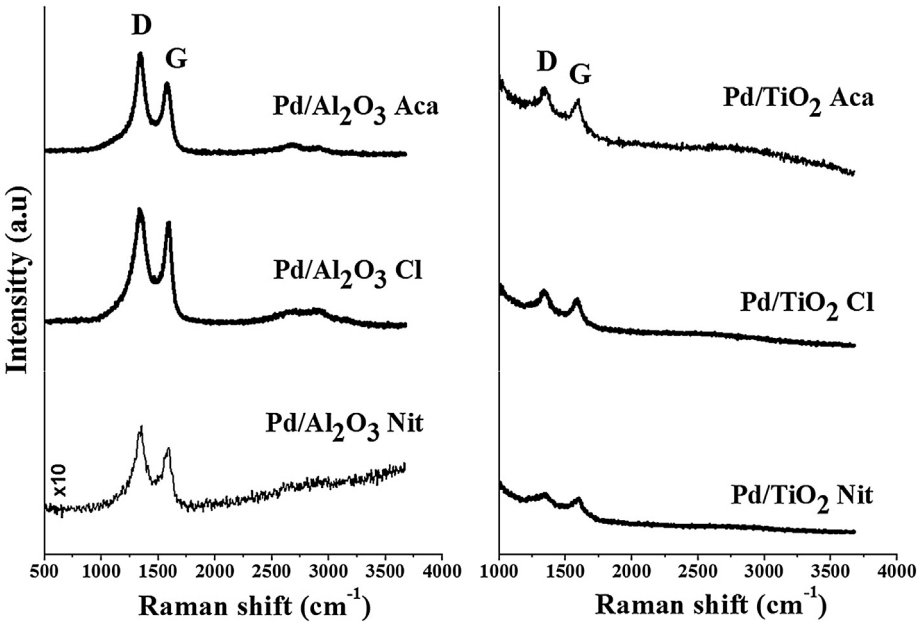

Fig. 12. Raman spectra of used palladium supported catalysts after acetic acid decomposition.

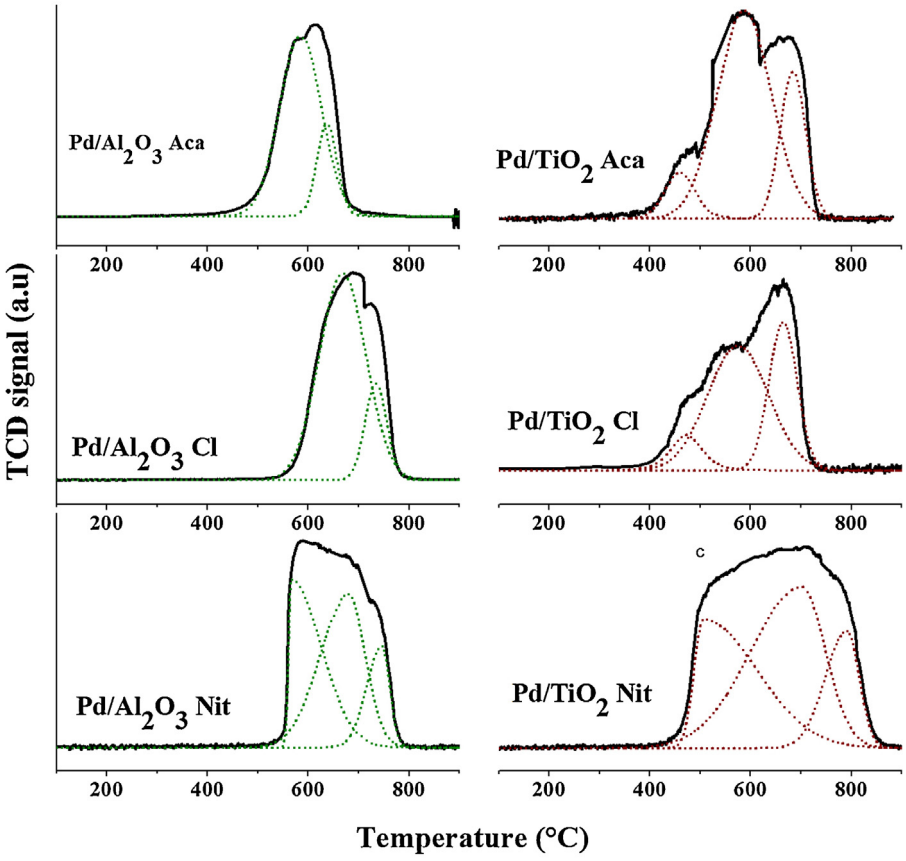

Fig. 13. TPO profiles of the carbon species present on supported palladium catalysts after acetic acid decomposition.

carbon structures, but D band was more intense, which indicate there was more disordered carbon than ordered carbon. For titania supported catalysts there were additional bands between 100 cm^{-1} and 700 cm^{-1} (not shown), which are attributed to the support, predominantly the anatase phase, which is in agreement with the XRD results of passivated titania supported catalysts [43]. Fig. 13 illustrates the TPO profiles due to the oxidation of carbon species produced on the supported palladium catalysts after decomposition of acetic acid. The Raman observations after the catalytic tests revealed two types of carbon (ordered and disordered) and in fact all the catalysts exhibited broad and not well-defined TPO peaks. Pd/TiO_2 Aca and Pd/TiO_2 Cl catalysts showed more clearly the presence of three different species of carbon because there were three shoulders at 480 °C, 585 °C and 670 °C in the large peak. The amount of carbon in the used samples is displayed in Table 5. Pd/Al_2O_3 Nit displayed the higher amount of deposited carbon (2.4 g/g_{cat}) followed by Pd/Al_2O_3 Aca > Pd/Al_2O_3 Cl > Pd/TiO_2 Nit > Pd/TiO_2 Aca > Pd/TiO_2Cl. The catalyst deactivation observed in the stability tests was attributed to the carbon deposits that cover the metallic particle and the support. Although Pd/Al_2O_3 Nit was the most active catalyst during the stability tests, loss of activity was observed due to formation of carbon deposits.

4. Conclusions

The use of different palladium precursors and mainly different supports played an important role on activities of the catalysts for acetic acid decomposition. Alumina supported catalysts were more active and selective on hydrogen than titania supported catalysts at higher temperatures. The present work shows that the decomposition of acetic acid over palladium supported catalysts can be performed with high activity at temperatures above 700 °C and palladium acetylacetonate is a suitable precursor of palladium catalysts for decomposition of acetic acid. This behavior was influenced by the different surface site composition depending on the used precursors. Pd/Al_2O_3 Nit is a suitable precursor for acetic acid conversion due to the presence of different coordination sites (Pd(100) and Pd(111)) which were responsible for the good activity, due to the higher presence of site defects that favored acetic acid dissociation as evidenced by the DRIFTS of adsorbed acetic acid experiments. On the other hand, for Pd/Al_2O_3 Aca catalyst only Pd(111) was observed which favored the good selectivity for hydrogen. TiO_2 supported catalysts showed SMSI behavior, causing an increase in the turnover frequency. DRIFTS results showed that acetate species were important on transformation of acetic acid and on hydrogen production, as evidenced on alumina supported catalysts. In the stability tests, all catalysts showed loss of activity with time due to the formation of carbon on their surfaces. The deposited carbon, for all catalysts, was a mixture of ordered and disordered carbon.

Acknowledgements

The authors are grateful to Capes, CNPq and Faperj for the financial support.

References

[1] G. Mao, H. Zou, G. Chen, H. Du, J. Zuo, Renew. Sustain. Energy Rev. 52 (2015) 1823–1833.
[2] S. Nanda, R. Azargohar, A.K. Dalai, J.A. Kozinski, Renew. Sustain. Energy Rev. 50 (2015) 925–941.
[3] F. Barbir, Energy 34 (2009) 308–312.
[4] J.D. Holladay, J. Hu, D.L. King, Y. Wang, Catal. Today 139 (2009) 244–260.
[5] S. Czernik, R. French, Int. J. Hydrogen Energy 39 (2014) 744–750.

[6] L. Garcia, R. French, S. Czernik, E. Chornet, Appl. Catal. A: Gen. 201 (2000) 225–239.
[7] L.M. Esteves, M.H. Brijaldo, V.M. Ribeiro, F.B. Passos, Rev. Virtual Quim. 6 (2014) 1062–1075.
[8] K.K. Pant, P. Mohanty, S. Agarwal, A.K. Dalai, Catal. Today 207 (2013) 36–43.
[9] K. Takanabe, K.I. Aika, K. Inazu, T. Baba, K. Seshan, L. Lefferts, J. Catal. 243 (2006) 263–269.
[10] X. Hu, G. Lu, J. Mol. Catal. A: Chem. 261 (2007) 43–48.
[11] C. Houtman, M.A. Barteau, Surf. Sci. Lett. 248 (1991) 57–76.
[12] J.L. Davis, M.A. Barteau, Surf. Sci. Lett. 256 (1991) 50–66.
[13] M. Bowker, C. Morgan, J. Couves, Surf. Sci. 555 (2004) 145–156.
[14] Y. Li, M. Bowker, J. Catal. 142 (1993) 630–640.
[15] C.J. Houtman, N.F. Brown, M.A. Barteau, J. Catal. 145 (1994) 37–53.
[16] E.W. Scharpf, J.B. Benziger, J. Phys. Chem. 91 (1987) 5531–5534.
[17] R.J. Madix, J.L. Falconer, a. M. Suszko, Surf. Sci. 54 (1976) 6–20.
[18] Z.F. Pei, V. Ponec, Appl. Surf. Sci. 103 (1996) 171–182.
[19] M.H. Brijaldo, H.A. Rojas, J.J. Martínez, F.B. Passos, J. Catal. 331 (2015) 63–75.
[20] M.J. MacCarrone, C.R. Lederhos, G. Torres, C. Betti, F. Coloma-Pascual, M.E. Quiroga, J.C. Yori, Appl. Catal. A: Gen. 441–442 (2012) 90–98.
[21] R. Monteiro, L.C. Dieguez, M. Schmal, Catal. Today 65 (2001) 77–89.
[22] C.L. Pieck, C.R. Vera, E.M. Peirotti, J.C. Yori, Appl. Catal. A: Gen. 226 (2002) 281–291.
[23] X. Wang, G. Wu, N. Guan, L. Li, Appl. Catal. B: Environ. 115–116 (2012) 7–15.
[24] W.J. Shen, M. Okumura, Y. Matsumura, M. Haruta, Appl. Catal. A: Gen. 213 (2001) 225–232.
[25] S. Scirè, S. Minicò, C. Crisafulli, Appl. Catal. A: Gen. 235 (2002) 21–31.
[26] L.M.T. Simplício, S.T. Brandão, E.A. Sales, L. Lietti, F. Bozon-Verduraz, Appl. Catal. B: Environ. 63 (2006) 9–14.
[27] N.M. Kinnunen, M. Suvanto, M.A. Moreno, A. Savimäki, K. Kallinen, T.-J.J. Kinnunen, T.A. Pakkanen, Appl. Catal. A: Gen. 370 (2009) 78–87.
[28] H.S. Fogler, Elements of Chemical Reaction Engineering, Prentice Hall, New Jersey, 1999.
[29] M. Hosseini, S. Siffert, H.L. Tidahy, R. Cousin, J. Lamonier, Cat. Today 122 (2007) 391–396.
[30] J.J. Dodson, H.E. Hagelin-weaver, J. Mol. Catal. A: Chem. 410 (2015) 271–279.
[31] K.S.W. Sing, D.H. Everett, R.A.W. Haul, L. Moscou, R.A. Pierotti, J. Rouquérol, T. Siemieniewska, Pure Appl. Chem. 57 (1985) 603–619.
[32] G. Neri, G. Rizzo, L. De Luca, A. Donato, M.G. Musolino, R. Pietropaolo, Appl. Catal. A: Gen. 356 (2009) 113–120.
[33] H. Rojas, G. Borda, P. Reyes, M. Brijaldo, J. Valencia, J. Chil. Chem. Soc. 56 (2011) 793–798.
[34] R.J. Liu, P.A. Crozier, C.M. Smith, D.A. Hucul, J. Blackson, G. Salaita, Appl. Catal. A: Gen. 282 (2005) 111–121.
[35] D.O. Simone, T. Kennelly, N.L. Brungard, R.J. Farrauto, Appl. Catal. 70 (1991) 87–100.
[36] F.B. Noronha, D.G.A. Aranda, A.P. Ordine, M. Schmal, Catal. Today 57 (2000) 275–282.
[37] M.G. Musolino, G. Apa, A. Donato, R. Pietropaolo, F. Frusteri, Appl. Catal. A: Gen. 325 (2007) 112–120.
[38] S. Bhogeswararao, D. Srinivas, J. Catal. 327 (2015) 65–77.
[39] N. Seshu Babu, N. Lingaiah, P.S. Sai Prasad, Appl. Catal. B: Environ. 111–112 (2012) 309–316.
[40] F. Cárdenas-Lizana, S. Gómez-Quero, M.A. Keane, Appl. Catal. A: Gen. 334 (2008) 199–206.
[41] F. Cárdenas-Lizana, S. Gómez-Quero, C. Amorim, M.A. Keane, Appl. Catal. A: Gen. 473 (2014) 41–50.
[42] F.B. Noronha, M.A.S. Baldanza, R.S. Monteiro, D.A.G. Aranda, A. Ordine, M. Schmal, Appl. Catal. 210 (2001) 275–286.
[43] L.M. Sikhwivhilu, N.J. Coville, D. Naresh, K.V.R. Chary, V. Vishwanathan, Appl. Catal. A: Gen. 324 (2007) 52–61.
[44] H. Karhu, A. Kalantar, I.J. Väyrynen, T. Salmi, D.Y. Murzin, Appl. Catal. A: Gen. 247 (2003) 283–294.
[45] H. Huang, D.Y.C. Leung, J. Catal. 280 (2011) 60–67.
[46] W. Rachmady, M.A. Vannice, J. Catal. 207 (2002) 317–330.
[47] S. Rieck, A.T. Bell, J. Catal. 54 (1987) 46–54.
[48] G. Blyholder, J. Phys. Chem. A 68 (1964) 2772–2777.
[49] A. Palazov, G. Kadinov, Ch. Bonev, D. Shopov, J. Catal. 74 (1982) 44–54.
[50] R. Haley, M. Tikhov, Catal. Lett. 76 (2001) 125–130.
[51] Z. Li, F. Calaza, F. Gao, W.T. Tysoe, Surf. Sci. 601 (2007) 1351–1357.
[52] A.R. Garcia, J.L. da Silva, L.M. Ilharco, Surf. Sci. 415 (1998) 183–193.
[53] M.A. Hasan, M.I. Zaki, L. Pasupulety, Appl. Catal. A: Gen. 243 (2003) 81–92.
[54] J. Xu, W. Zhou, Z. Li, J. Wang, J. Ma, Int. J. Hydrogen Energy 34 (2009) 6646–6654.
[55] J.E. Herrera, D.E. Resasco, J. Catal. 221 (2004) 354–364.

Please cite this article in press as: L.M. Esteves, et al., J. Mol. Catal. A: Chem. (2016), http://dx.doi.org/10.1016/j.molcata.2016.02.001